IoT-Based Interdigital Capacitance Sensing System for Damage Detection in CFRP-Concrete Structures

MOHAMED ABDELRAHEEM[1], **(Member, IEEE),**
MAHMOUD ABDELHAFEEZ[1], **(Student Member, IEEE),**
AND AMR NASSR[2,3]
[1]Electrical Engineering Department, Assiut University, Assiut 71515, Egypt
[2]Civil Engineering Department, Assiut University, Assiut 71515, Egypt
[3]Sustainable Design Engineering, Universities of Canada in Egypt, Cairo 11371, Egypt
Corresponding author: Mohamed Abdelraheem (m.abdelraheem@aun.edu.eg)

ABSTRACT In this paper, we present an Internet of Things framework for structural health monitoring. The proposed system detects the delimitation and debonding in composite concrete structures: more specifically, develop an IoT-Based Non-Destructive Test (NDT) to detect debonding between Carbon Fiber sheets and Concrete slabs. An Inter Digital Capacitance Sensor is designed and fabricated to function as the primary detection element. The sensor is embedded within an IoT node that manages the measurement process, captures the measurement location automatically, and performs essential data filtering operations with an attached graphical interface that allows basic control and early-access to the measured data. The IoT node integrates within the larger framework via wireless WiFi connection throughout which the data is transferred and control functions are administrated. The paper presents the system design details including mathematical modeling for the capacitance sensing element, finite element simulation results, and practical setup measured data.

INDEX TERMS Structural health monitoring, inter digital capacitance sensor, Internet of Things.

I. INTRODUCTION

Wet laminated composites, e.g., Fiber Reinforced Polymers (FRP), are widely employed to concrete structures to enhance its strength and repair deteriorated elements. These composites replace the conventional materials because of their lightweight, resistance to corrosion, and extended strength. One important factor for these composites to be effective is the good adhesiveness to the concrete surface. Different types of damages can occur to composites during or after installation like debonding, delamination, or fiber breakage which would considerably degrade its performance [1], [2]. Therefore, the detection of such imperfections is crucial task in structural health monitoring (SHM) activities for enhancing and ensuring the safety of such concrete structures. Numerous Non-Destructive Testing (NDT) techniques were developed to detect imperfections in FRP-concrete structures. Active

thermography techniques were used in the literature to detect debonding and rebar locations in concrete structures by heating the sample under inspection and using external energy source, e.g., microwaves, and then detecting the thermal properties variations across the surface of the sample using infrared camera [3], [4]. Similarly, radiography was also used in SHM utilizing penetrating electromagnetic waves [5], [6]. Gamma or X-rays is transmitted from a radiation source into the structure penetrating it, then the rays are received from the other side of the structure using a radiation sensitive sensing receptor for analysis. Capacitive sensing techniques were also used to detect different types of damages in concrete structures [7], [8] or for the detection of rebars [9]. The capacitive sensing methods implied measuring and scanning the capacitance formed on coplanar electrodes sensor placed on contact with the concrete structure surface. Detection of damages depends on capacitance variation, as the locations of damages (or rebars) give different capacitance values compared to other plain or normal locations. Additionally,

The associate editor coordinating the review of this manuscript and approving it for publication was Zhenhui Yuan.

acoustic waves were also used as NDT technique in the form of ultrasonic waves for various SHM tasks in concrete structures. For example, it was used for examining the rebars status [10]–[12], for the assessment of concrete structures [13], [14], detection of damage in concrete [15]–[17] and in estimating the mixing ratio between water and concrete [18], [19]. Moreover, the Ground Penetrating Radar (GPR) is used as a single-sided NDT technique for SHM. Similar to ultrasonic waves but with different type of waves, GPR technique depends on transmitting an electromagnetic pulse with high frequency into the concrete structures and then receives the scattered wave back. Different types of damages, existence of rebars, or any other aspect that leads to a change in the dielectric signature of the tested material will result in a measurable signature in the reflected wave which is used as a detection sign. Low-frequency techniques also exist like eddy current based methods [20]–[23]. In this method, an excitation coil generates a magnetic field that produces eddy current through the sample under investigation. These currents produce, in turn, a magnetic field that is picked up by another pick-up coil. The presence of damages or rebars in the concrete affects the magnetic field sensed by the pick-up coil which is the basis of the detectability of this method.

While the above-mentioned NDT systems/techniques for SHM achieve good results for detection of different types of damages in concrete structures, they have some disadvantages. Some of these systems are complex and pricy like GPR, others resemble bad effects on health like radiography. Some techniques require highly qualified operators like ultrasonic methods. Despite the simplicity and efficiency of capacitance methods, they are not developed as a complete system i.e. they require manual positioning, measurements, and analysis of data in order to produce results. In addition, the aforementioned systems, for approaches that actually support a complete system, are local i.e. the collected data are processed in a nearby computer where the results are also produced. Besides utilizing wired connections between the sensors and the processing unit, these systems don't support data transmission for far central units for further processing based on multiple source data aggregation.

Internet of Things (IoT) technology provides a solution for the above-mentioned challenge. In IoT paradigm, the devices ''things'' are powered with communication modules to allow them to communicate with each other and/or with cloud services [24]. Typical SHM system consists of three subsystems, namely, sensing and data acquisition subsystem, management subsystem, and data access and retrieval subsystem [25]. IoT technology combines these three systems in an automated way which makes IoT an emerging technology for SHM service. Many IoT-based SHM systems have been developed in the past decade. In [26], the authors developed an SHM system using TCP/IP network over Bluetooth technology. The vibration signals measured at different points of the monitored bridge, using accelerometer sensors, are transmitted to a central server where the structure natural frequencies and mode shapes are obtained. Authors of [27] present a

mathematical model that can be integrated with an IoT platform like Raspberry Pi to detect the size and location of damages in steel plate using guided wave using piezoelectric transducers. In [28], the authors designed and implemented a general SHM based on IoT using LabVIEW platform. The structure condition is assisted by collecting a set of sensing data like temperature, pressure and vibration. the collected data are transmitted to a processing server run LabVIEW using GPRS module. A low-cost and flexible IoT-based platform for bridge health monitoring is presented in [29]. The vibration signals are transmitted form the Arduino Uno based IoT node using WiFi modules to a remote server over the internet. The server hosts a web API that enable the user to access the vibration data in a real time fashion. The system was validated on a crack and un-cracked beam where the natural frequencies of both specimens are obtained and visualized on the web interface. Sensors fusion technology is also integrated with IoT for SHM. In [30] a complete IoT system which integrates multiple sensors for different phenomena like tilt, shock, strain, vibration, temperature, and humidity for monitoring structural condition is presented. The Sensors data are transmitted via WiFi module to an open-source cloud platform. The design feature low cost and low power profile. The system has been evaluated on a steel pedestrian staircase where different sensors data have been integrated to obtain the structure condition. NGS-PlantOne system, a specially designed IoT for pervasive monitoring of industrial machinery is presented in [31]. This system is implemented in a power plant where 33 IoT nodes equipped with temperature or accelerometer sensors are used. The nodes communicate with gateways using IEEE802.15.4, 6LoWPAN communication technology. The gateway relays the sensing data through Ethernet network to a central server where the data are visualized. Early warning system can benefit from the integration between SHM and IoT technologies. In [32] an early warning system is presented based on IoT technology. Data from stress gauge, earth pressure cell and inclinometer are collected and transmitted to a central warning system where different warning categories are defined according to the structure status. The system has been validated on an excavation pit structure.

In this paper we present a complete IoT based system for damage detection, more specifically, debonding in FRP structures. We start by modelling the Inter Digital capacitance sensor (IDCS) mathematically with the presence of a layered dielectrics material (CFRP sheets, air gap, and the concrete). Then, a Finite Element Model (FEM), for the same theoretical setup, is simulated and the resulted capacitance values were compared to those of the theoretical model for validation. To automate the detection process, we designed an IoT based capacitance measuring system using the IDCS sensor, processing unit (microcontroller), communication module (WiFi), optical movement sensor to automatically record the sensor position and a graphical screen for control and capacitance values and position display.

Fig. 1 shows an overview of the proposed system. The measured capacitance value is displayed on a graphical display

and/or transmitted to a local or cloud based server where the capacitance value is stored and visualized to emphasis any debonding in the monitored structure. Finally, we cast a concrete slab with artificial air voids and cover it with epoxy coated Carbon-fiber-reinforced polymer. The casted slab was used to practically benchmark the designed system features and capabilities. It was also used to provide practically measured data for comparison and confirmation with the mathematical and the simulation models.

Paper Organization –The rest of the paper is organized as follows. The theoretical background is presented in Section II. The Finite Element simulation is introduced in Section III. Section IV describe the proposed IoT system. The practical system is presented in Section V. The paper is concluded in Section VI.

II. THEORETICAL BACKGROUND
The proposed detection methodology relies on sensing the variation of the dielectric signature of the material compositions of CFRP-concrete constructions. At uniform locations of the material, i.e. locations without damage or compositions disturbance, the dielectric constant would be also uniform. However, at locations of the localized damages there would be disturbance in the dielectric constants and the resulting dielectric signature at this location. A disturbance in the dielectric signature at some location, in turn, can be sensed and quantified as a variation in the capacitance measured at that location compared to other uniform locations.

The coplanar IDCS structure is adopted to measure the capacitance across the surface of the material under inspection. As can be inferred from Fig. 2, the IDCS consists of two groups of interlocked metallic fingers parallel to each other. The two groups have opposite voltage polarity and capacitance is formed between them.

The fingers are assumed to have the same width of w and gap distance between any two consecutive fingers is g. The fingers have a length of L which is considered long enough to make fringing effects negligible. The conformal mapping approach [33] can be used to deduce analytical

expressions that express the coupling and other electrical properties of coplanar electrodes. Research conducted by Igreja and Dias [33], [34] demonstrated the application of conformal mapping approach and the partial capacitance method to calculate the capacitance of IDCS structure embedded in multi-layers dielectric slabs with semi-infinite nature. In their research, the capacitance was calculated in case of the dielectric constant being varied monotonically between the dielectric layers i.e. either increasing or decreasing all the way. So, the results of this study cannot be applied when the dielectric constant is changed arbitrarily between the layers. After that, Blume *et al.* [35] adopted the Schwarz-Christoffel conformal mappings (SCM) and manipulated the partial capacitance approach of [34] and [35] to be able to calculate the capacitance of IDCS structure embedded in multi-layer dielectric slabs with arbitrary changing dielectric constant. In this paper, the approach of [35] is followed to calculate the capacitance of the IDCS placed on the material compositions of CFRP concrete constructions.

A cross section of the proposed model of the IDCS and the dielectric layers is presented in Fig. 3. Each two consecutive fingers have opposite voltage applied and, hence, a zero potential wall is formed between them. The capacitance formed between an inner finger and the nearby zero-potential wall is called inner cell capacitance C_i and the capacitance formed between an external finger and the zero potential wall is called external cell capacitance C_E. The dielectric layers are assumed to be isotropic i.e. the dielectric constant is constant across the layer and changes only across the interface

FIGURE 2. Inter digital capacitance sensor (IDCS) structure.

FIGURE 3. IDCS model presenting different capacitance components.

TABLE 1. Cell constant k_{cell}^c for the case of exterior cell.

Finite height layer SPC	Finite height layer PPC	Infinite height layer
$k = \sqrt{\frac{t_B - 1}{t_A - 1}}$	$k_{cell}^c = \frac{K(k')}{K(k)}$ where $k = \sqrt{\frac{t_A(t_B-1)}{t_B(t_A-1)}}$	$k = \sqrt{t_B + 1}$
$t_A = \cosh^2\left(\frac{\pi(1+\eta)}{2r}\right)$		$t_B = -\frac{4\eta}{(\eta+1)^2}$
$t_B = \cosh^2\left(\frac{\pi(1-\eta)}{2r}\right)$		
in case of $r \to 0$		
$k_{cell}^c = \frac{2\eta}{r} + 1$	$k_{cell}^c = \frac{r}{1-\eta}$	

between the layers. The change in the dielectric constant is arbitrary i.e. not necessary monotonic. It should be noted that the heights of the different layers are all measured from the IDCS surface and that the model assumes an open configuration i.e. the height of the last layer extends to infinity. Based on the capacitance components distribution shown in Fig. 3 the total capacitance for an N finger IDCS is calculated as:

$$C_T = (N-3)\frac{C_I}{2} + 2 \cdot \frac{C_I \cdot C_E}{C_I + C_E} \tag{1}$$

The following geometrical non-dimensional parameters will be used through the calculations of capacitance components:

$$\eta = \frac{w}{w+g} \tag{2}$$

and

$$r = \frac{2h}{w+g} \tag{3}$$

It should be noted that the total capacitance formed on the IDCS will be the sum of the capacitances corresponding to layers above and below the sensor. i.e. the approach has to be applied twice, once for each half space, and the results should be summed. In case of monotonically changing dielectric constant, the partial capacitance approach can be applied to calculate the capacitance formed on the IDCS using the parallel plate capacitance (PPC) in case of increasing dielectric constant or the series plate capacitance (SPC) in case decreasing dielectric constant [36], where the calculations are based on [37]–[40]. For the PPC case with n dielectric layers, the cell capacitance C_{cell} (internal or external) can be calculated as:

$$C_{cell} = L\left[\sum_{i=1}^{n-1}(\epsilon_i - \epsilon_{i+1})\,k_{cell}^c(\eta, r_i) + \epsilon_n k_{cell}^c(\eta, r_n)\right], \tag{4}$$

and in case of SPC:

$$C_{cell} = \frac{1}{L}\left[\sum_{i=1}^{n-1}\left(\frac{1}{\epsilon_i} - \frac{1}{\epsilon_{i+1}}\right)\frac{1}{k_{cell}^c(\eta, r_i)} + \frac{1}{\epsilon_n}\frac{1}{k_{cell}^c(\eta, r_n)}\right] \tag{5}$$

where ϵ_i is the electric permittivity of layer i, k_{cell}^c is a constant that depends on the configuration type: PPC or SPC, the geometry parameters η and r, and the cell type if it is
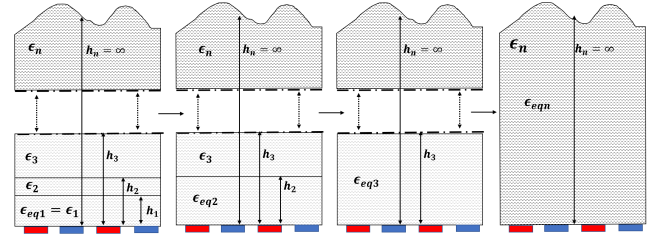
FIGURE 4. Repeated merging technique for cell capacitance calculation.

an internal or external cell. In [35], it was found that for two layers i and $i-1$, they can be merged together in a single layer i with height h_i and equivalent permittivity:

$$PPC: \epsilon_{eq,i} = \left(\epsilon_{eq,i-1} - \epsilon_i\right)\frac{k_{cell}^c(\eta, r_{i-1})}{k_{cell}^c(\eta, r_i)} + \epsilon_i \tag{6}$$

$$SPC: \epsilon_{eq,i} = \frac{\epsilon_{eq,i-1}\epsilon_i k_{cell}^c(\eta, r_{i-1})}{k_{cell}^c(\eta, r_i)\left(\epsilon_i - \epsilon_{eq,i-1}\right) + \epsilon_{eq,i-1}k_{cell}^c(\eta, r_{i-1})} \tag{7}$$

where in case of the first layer above the electrodes $\epsilon_{eq,1} = \epsilon_1$. The approach of [35] depends on merging the lowest two layers into equivalent layer, then repeating the process between the resultant equivalent layer and the layer above it to get a new equivalent layer and so on. The process is repeated till all the layers are merged into one equivalent layer with equivalent electric permittivity ϵ_n and height $h_n = \infty$ (assuming the open configuration i.e. the last layer extends to infinity). Fig. 4 describes the process of repeated merging. After merging all the layers into one equivalent layer, the cell capacitance can then be calculated by

$$C_{cell} = \epsilon_{eq,n} \cdot L \cdot k_{cell}^c(\eta, \infty). \tag{8}$$

Choosing to calculate the equivalent electric permittivity between two layers using the PPC or SPC equations depends on if the electric permittivity is increasing at the boundary between the two layers or decreasing. If $\epsilon_{eq,i-1} < \epsilon_i$ this means the electric permittivity is increasing at the boundary and hence the SPS equation should be used. But if $\epsilon_{eq,i-1} > \epsilon_i$ then PPC equation should be used to calculate the effective permittivity of the two layers as the electric permittivity decreases across the boundary. The equations to calculate the cell constant $k_{cell}^c(\eta, r_i)$ in case of exterior cell are in Table 1 while those for interior cells are in Table 2 [35],
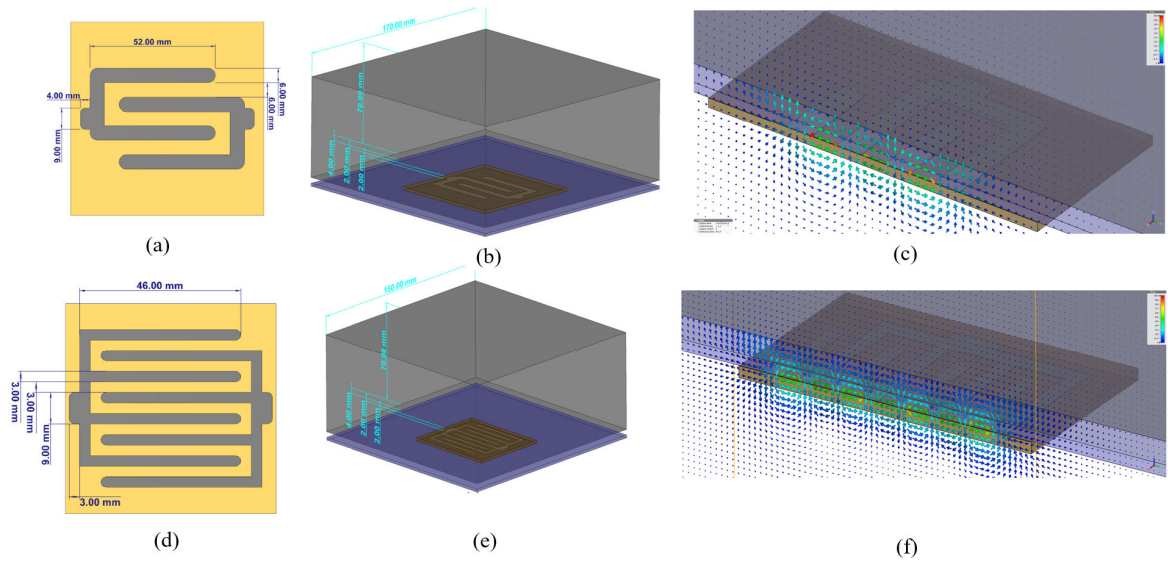
FIGURE 5. (a) IDCS dimension (b) FE model setup (c) electric field distribution for 4 Finger variant. (d) IDCS dimension (e) FE model setup (f) electric field distribution for 8 Finger variant.

TABLE 2. Cell constant k_{cell}^c for the case of interior cell.

Finite height layer (SPC)	Finite height layer (PPC)	infinite height layer
$k_{cell}^c = \frac{K(k_w)}{K(k'_w)}$	$k_{cell}^c = \frac{K(k'_w)}{K(k_w)}$	$k_{cell}^c = \frac{K(k')}{K(k)}$
Where		
$k_w = \sqrt{\frac{(k+1)(1+t_B)}{2(1+kt_B)}}$	$k_w = \sqrt{\frac{(k+1)(1-t_B)}{2(1-kt_B)}}$	$k = \sqrt{t_B+1}$
$t_B = sn\left(K(k)(2\eta-1),m\right),\ \ m = k^2$		
$k = \left(\frac{\vartheta_2(0,q)}{\vartheta_3(0,q)}\right)^2$		$t_B = \sinh^2\left(j\frac{\pi\eta}{2}\right)$
$q = e^{-2\pi r}$		
in case of $r \to 0$		
$k_{cell}^c = \frac{\eta}{2}+\frac{1}{2}$	$k_{cell}^c = \frac{1}{2}\left(\frac{r}{1-\eta+r}+\frac{r}{1-\eta}\right)$	

where $K(k)$ is the complete elliptic integral of the first kind, and $k' = \sqrt{1-k^2}$. In case of interior cell, $\vartheta_2(0,q)$ and $\vartheta_3(0,q)$ are the Jacobi theta functions of second and third type, respectively and $sn(x,m)$ is the Jacobi elliptic sine function. Authors of [35] also noticed that when for the values of $r < 0.05$ the cell constants are better approximated by the relations in the last rows in Tables 1 and 2 for the case of exterior and interior cell respectively.

III. FINITE ELEMENT SIMULATION

The 3D models in this study have been constructed using Simula CST Studio Suite electrostatic solver [41]. The finite element simulation is electrostatics, which is adequate for the low operating frequency of IDCS. Fig. 5 shows the FE models for two IDCS configurations (IDCS1 of 4 fingers and IDCS2 of 8 fingers) and their electric field distribution. The composite retrofitted concrete system has been modeled as two layers of different dielectric permittivities. Depending on fiber content in CFRP, the dielectric permittivity of CFRP is specified according to [37]. The electric field immediately at the sensor is the highest and decreases exponentially away from there. Because this region is where defects studied are

typically located (i.e. immediately under the composite layer rather than deep inside the concrete substrate), the proposed IDCS is highly sensitive to any change in the material composition or dielectric properties. Fig. 6 (a) and (b) shows the capacitance measurements (mathematically and by simulation) obtained from IDCS1 and IDCS2 for air void defects, respectively. The measured capacitance values are affected by the presence of air voids, as the capacitance decreased exponentially with increasing the air void gap distance. The gap distance = 0 represents the case of full or healthy bond (no defects). The decrease in the output signals is attributed to the low value of the dielectric permittivity of air, compared to that of the concrete. The IDCS had an asymptotic response for defect heights more than 2 *mm* for sensors of 4 fingers and 1 *mm* for sensor of 8 fingers. From Fig. 5 it can be seen that the 4 fingers sensor shows better detection sensitivity and depth than the 8 fingers sensor. This is because the 8 fingers sensor shows higher average capacitance levels compared to the 4 fingers one, which can be inferred from the capacitance values of the 8 fingers sensor being almost double of its 4-fingers counterpart. It should be noted that the capacitance levels/ranges are not dependent on the sample but on the sensor construction itself. The 8 fingers sensor presents higher levels because of the higher number of fingers and closer distance between the fingers. A sensor that proposes lower capacitance levels is better, because the fluctuation of the measured capacitance around these levels will be more sensible. For this reason, the 4 fingers sensors will be used in the rest of the paper.

IV. IoT SYSTEM FOR DAMAGE DETECTION

In this section we introduce the details about the design and operation of the IoT node for structural health monitoring.
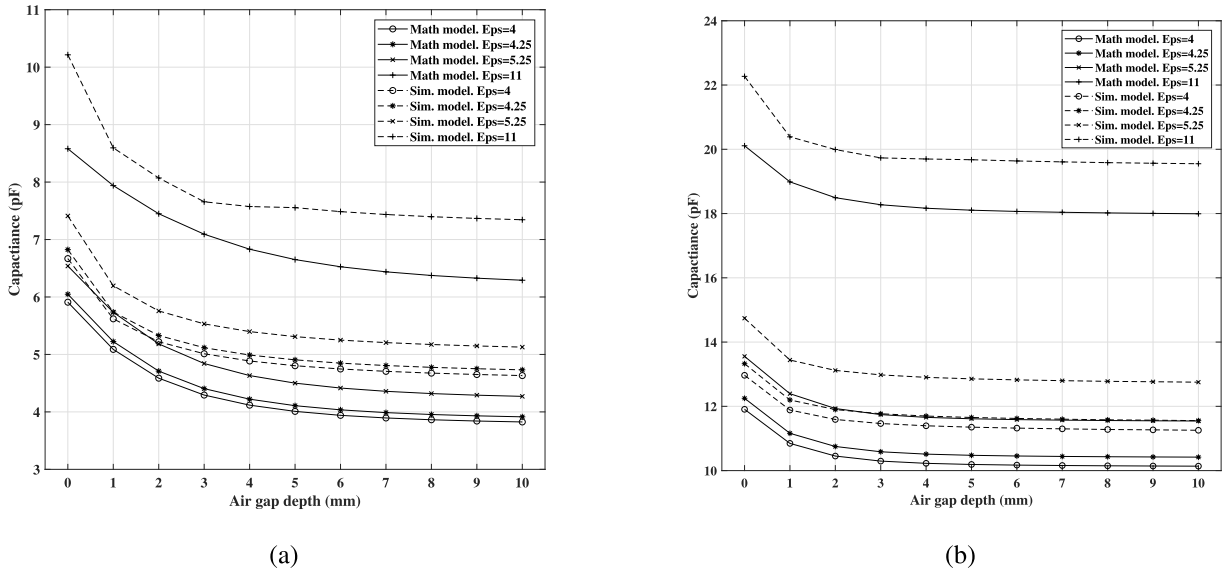
FIGURE 6. Capacitance response with air gap depth for (a) IDCS 1 (4 fingers) (b) IDCS 2 (8 fingers).

The The main components of the system are:

- Central unit (Arduino Duo)
- Capacitance measurement circuit
- Movement detection mechanism (Optical Sensor)
- Wireless transmission module (ESP8266 -12E WiFi Module [42])
- In-device user interface (Graphical Touch screen)
- Web interface

A. CENTRAL UNIT

Arduino Due used as controller of this project. It based on Atmel SAM3 × 8E ARM Cortex-M3 32 bit microcontroller [43], it has 4 UARTs (hardware serial ports) and an USB OTG capable connection that fulfil the project requirements. The main function of the microcontroller is to manage capacitance measure circuit, movement detection sensor and wireless transmission process. The microcontroller runs on a 84MHz clock makes it suitable for accurate calculations of the capacitance. We designed a dedicated shield on a Printed Circuit Board (PCB) to help implement the capacitance measurement circuit.

B. CAPACITANCE MEASUREMENT CIRCUIT

The voltage formed on a capacitor due to charging it with a dc voltage source through a resistor, can be calculated according as;

$$V_c(t) = v_f + (v_i - v_f) \cdot e^{\frac{-t}{RC}}. \tag{9}$$

where $V_c(t)$ is the voltage on the capacitor as a function of time t, v_f is the dc source output voltage, v_i is the initial voltage on the capacitor, R is the charging resistor value, and C is the capacitor value. Since the measurement mechanism ensures the capacitor is fully discharged at the beginning of the measurement cycle, V_i is assumed to be 0. So, (9) can be

reduced to:

$$V_c(t) = v_f(1 - e^{(\frac{-t}{RC})}), \tag{10}$$

and the capacitance can be written as:

$$c = \left(\frac{-t}{R}\right) \left(\frac{1}{\ln(1 - \frac{v_c(t)}{v_f})}\right). \tag{11}$$

At the start of measurement process the capacitor is not charged (empty) then it starts to charge through 3.3v applied to the resistor R from Arduino Due digital pin (V_{ref}). The capacitor voltage measured continuously by the Arduino ADC module pin, when the capacitor voltage reach specific value called (V_{ratio}) Arduino due raises interrupt and cach timer value T at the moment. Consider the capacitor (C) take time (T) to charge to voltage value (V_{ratio}) with the charging voltage V_{ref}, then we can calculate the capacitance from (11) as:

$$c = \left(\frac{-T}{R}\right) \left(\frac{1}{\ln(1 - \frac{v_{ratio}}{v_{ref}})}\right) \tag{12}$$

C. MOVEMENT DETECTION SENSOR

ADNS 3050 Optical movement sensor [44] is used to detect movement of the device, the sensor connected to Arduino due using USB OTG interface. The Arduino due calculates the change in the device position by calculating the relative displacement from a starting reference point and evaluating the position of the device in Cartesian coordinates (x, y) where x and y represent the horizontal and vertical position of the sensor in cm on the scanned surface relative to the reference starting point. The resolution of the sensor is 402 pixel/cm.
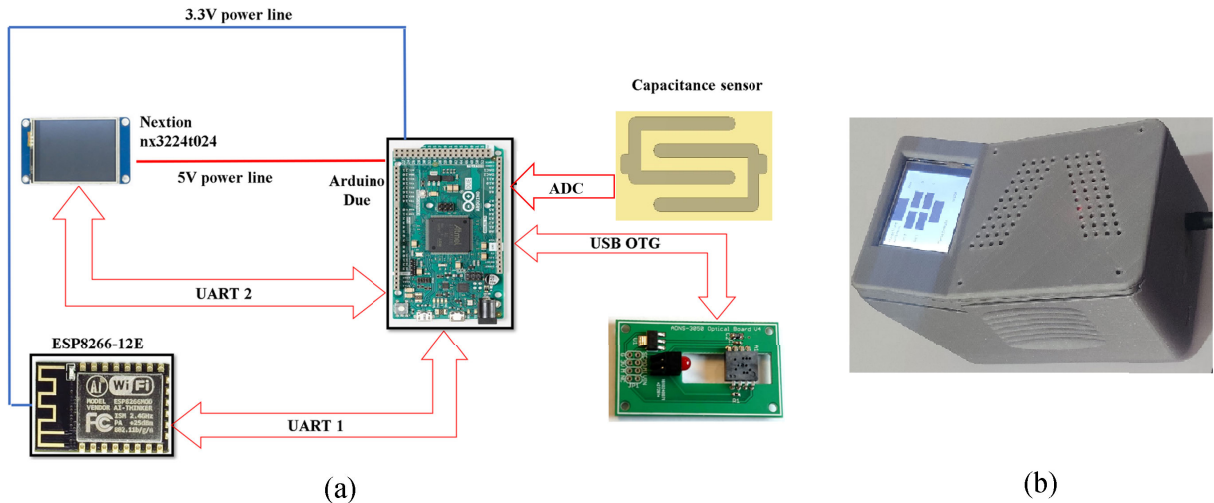
FIGURE 7. (a) Block diagram of the IDCS based IoT node (b) The final package of the node.

D. WIRELESS DATA TRANSMISSION

Measured capacitance and the detected position sent to TCP server using Wi-Fi module ESP8266 -12E connected through Arduino due UART interface. The TCP server created using Python code that connects to Wi-Fi module through internet network, receive measured data and record it to be sent to web page.

E. USER INTERFACE

This project provides easy and simple human interface using 3 inch graphical touch screen. The device has 2 measurement modes:

- Auto mode: start to measure capacitance once the movement detection sensor detect change in position, the measured capacitance and the position displayed at the screen using Arduino Due Serial 2.
- Manual mode: start to measure manually by pressing (Start) button and enter the position manually by increasing the (X) and (Y) values manually using the screen, measured capacitance displayed on the screen.

F. WEB INTERFACE

The system provides a centralized server with web interface to store and display the measured data. The server is based on two layer:

1) User Layer: Based on HTML and CSS, this layer is responsible of the user interface and chart displaying.
2) Core layer: Contains the TCP listener and database to receive the data from the IoT node store it in comma separated file.

The architecture of the server and it connection to the IoT node is depicted on Fig. 8.

The IoT node sends to the server the capacitance data with the corresponding coordinated to the server via TCP/IP
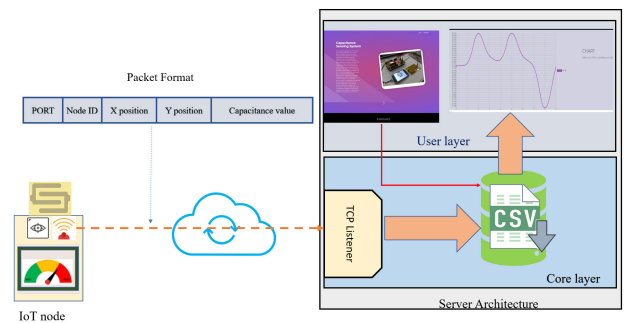

FIGURE 8. The central server architecture and packet format.

using its WiFi interface. After the data reception is completed, the server plots it on the web-page interface.

V. PRACTICAL EXPERIMENT

A concrete slab has been casted including virtual air gaps (grooves) with different depth (2 *mm*, 4 *mm*, and 6 *mm*) to represent the debonding effect between CFRP and the concrete surface. Fig. 9 (a) shows the actual casted concrete specimen with the created gaps. Fig. 9 (b) shows the slab after being covered with the CFRP. A cross section of the slab at plan A is shown in Fig. 9 (c). The IDCS was manufactured on a PCB form as shown in Fig. 9 (d).

The slab was scanned using the IoT node across the common center of the grooves (blue dashed line in Fig. 9 (a)) to cover all grooves and a healthy part. To assess the system repeatability the scan was repeated 5 times and the results with 95% is plotted in Fig. 10. As can be inferred from the beneath, the sensing technique is able to detect the air gaps beneath the CFRP (the debonding areas).
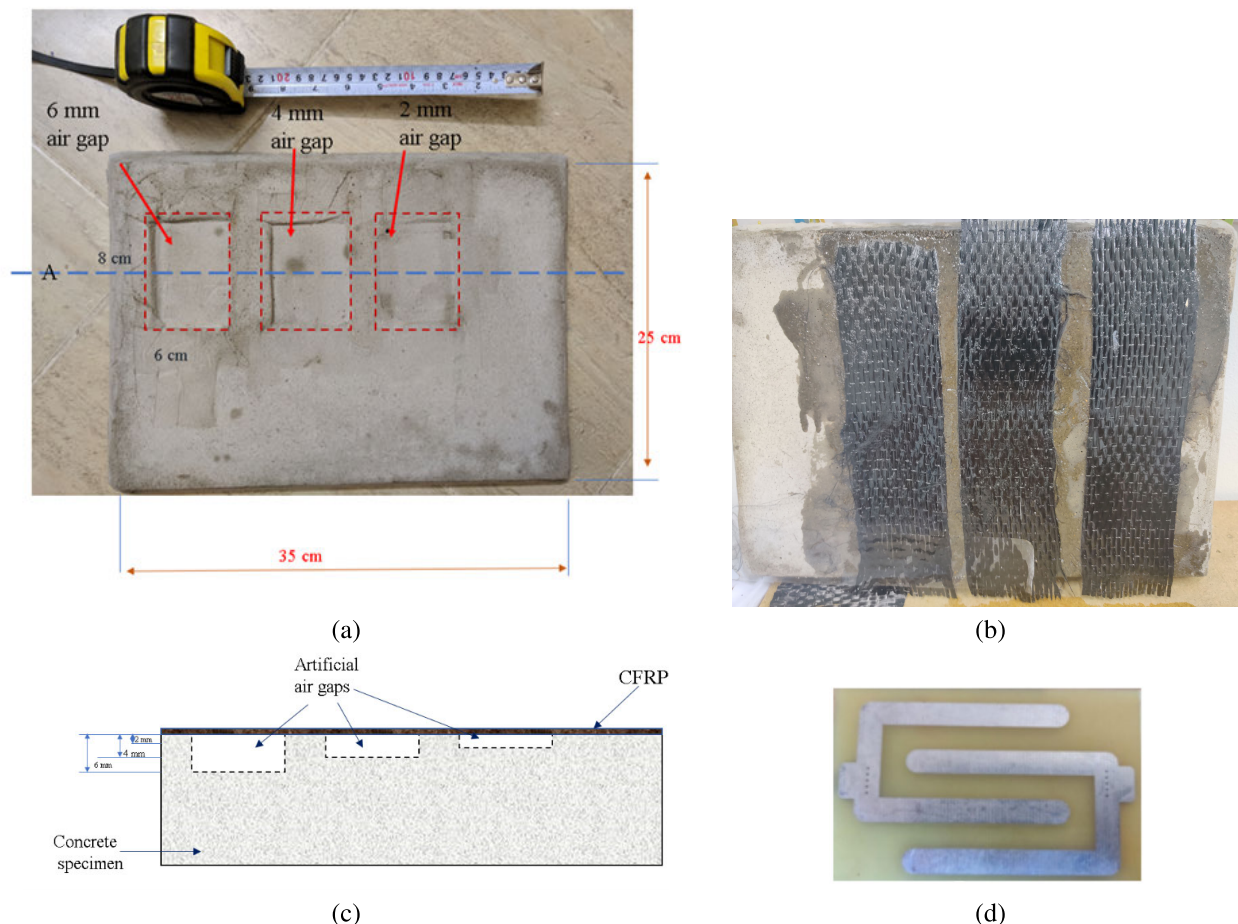
(a)

(b)

(c)

(d)

FIGURE 9. (a) The casted concrete slab with grooves shown the different dimensions (b) The slab covered with CFRP (c) cross section in the slab along the A plan (d) IDCS on its PCB form.
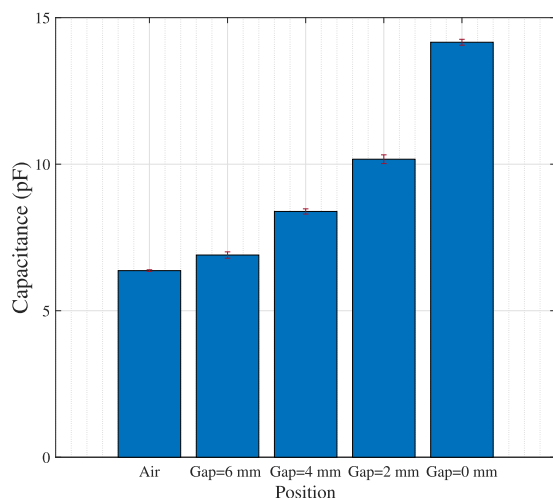

FIGURE 10. The measured capacitance at different points.

As can be inferred form the Fig. 10, which is also confirmed by the simulation and mathematical derivation. The system is able to distinguish between the healthy bond and

that with air gap between the CFRP and concrete. However, it is not able to measure the gap depth between the CFRP sheet and the concrete surface reliably.

VI. CONCLUSION

This paper presented an IoT system for damage detection in CFRP-concrete structure. The system depends on sensing the change of the dielectric properties when debonding occurs between the CFRP sheets and concrete surface using IDCS. A complete system was developed to automate the measuring, data transmission/storage, and data visualization. We augment the study by presenting a mathematical, numerical simulation comparison and practical experiment. The results prove the ability of the proposed system to detect the presence of debonding in CFRP-concrete structure. However, the ability of the system to characterize the gap between the CFRP sheets and the concrete surface is limited.

REFERENCES
[1] N. Toyama, Y. Kikushima, and J. Takatsubo, "Effect of delamination on lamb wave velocity in cross-ply laminates," *J. Mater. Sci. Lett.*, vol. 21, no. 24, pp. 1891–1893, 2002.

[2] M. Parlapalli and D. Shu, "Buckling analysis of two-layer beams with an asymmetric delamination," *Eng. Struct.*, vol. 26, no. 5, pp. 651–658, Apr. 2004.

[3] N. Makul, P. Rattanadecho, and D. K. Agrawal, "Applications of microwave energy in cement and concrete—A review," *Renew. Sustain. Energy Rev.*, vol. 37, pp. 715–733, Sep. 2014.

[4] F. Brachelet, S. Keo, D. Defer, and F. Breaban, "Detection of reinforcement bars in concrete slabs by infrared thermography and microwaves excitation," in *Proc. Int. Conf. Quant. Infr. Thermography*, 2014, pp. 1–8.

[5] H. E. Martz, G. P. Roberson, M. F. Skeate, D. J. Schneberk, and S. G. Azevedo, "Computerized tomography studies of concrete samples," *Nucl. Instrum. Methods Phys. Res. B, Beam Interact. Mater. At.*, vol. 58, no. 2, pp. 216–226, 1991.

[6] H. E. Martz, D. J. Schneberk, G. P. Roberson, and P. J. M. Monteiro, "Computerized tomography analysis of reinforced concrete," *ACI Mater. J.*, vol. 90, no. 3, pp. 259–264, 1993.

[7] A. A. Nassr and W. W. El-Dakhakhni, "Damage detection of FRP-strengthened concrete structures using capacitance measurements," *J. Composites Construct.*, vol. 13, no. 6, pp. 486–497, Dec. 2009.

[8] A. A. Nassr and W. W. El-Dakhakhni, "Improved interdigital sensors for structural health monitoring of composite retrofit systems," *J. Reinforced Plastics Compos.*, vol. 30, no. 7, pp. 621–629, 2011.

[9] M. Abdelhafeez, A. A. Nassr, and M. Abdelraheem, "Capacitance-based technique for detection of reinforcement bars in concrete structures," *IEEE Sensors J.*, vol. 21, no. 6, pp. 7713–7724, Mar. 2020.

[10] H. W. Chung, "Effects of embedded steel bars upon ultrasonic testing of concrete," *Mag. Concrete Res.*, vol. 30, no. 102, pp. 19–25, Mar. 1978.

[11] B. L. Ervin, D. A. Kuchma, J. T. Bernhard, and H. Reis, "Monitoring corrosion of rebar embedded in mortar using high-frequency guided ultrasonic waves," *J. Eng. Mech.*, vol. 135, no. 1, pp. 9–19, Jan. 2009.

[12] H. W. Song and V. Saraswathy, "Corrosion monitoring of reinforced concrete structures—A," *Int. J. Electrochem. Sci*, vol. 2, pp. 1–28, Apr. 2007.

[13] J. S. Popovics and J. L. Rose, "A survey of developments in ultrasonic NDE of concrete," *IEEE Trans. Ultrason., Ferroelectr., Freq. Control*, vol. 41, no. 1, pp. 140–143, Jan. 1994.

[14] H. N. Tomsett, "The practical use of ultrasonic pulse velocity measurements in the assessment of concrete quality," *Mag. Concrete Res.*, vol. 32, no. 110, pp. 7–16, Mar. 1980.

[15] J.-F. Chaix, V. Garnier, and G. Corneloup, "Concrete damage evolution analysis by backscattered ultrasonic waves," *NDT E Int.*, vol. 36, no. 7, pp. 461–469, Oct. 2003.

[16] A. A. Shah, Y. Ribakov, and S. Hirose, "Nondestructive evaluation of damaged concrete using nonlinear ultrasonics," *Mater. Design*, vol. 30, no. 3, pp. 775–782, Mar. 2009.

[17] S. Ould Naffa, M. Goueygou, B. Piwakowski, and F. Buyle-Bodin, "Detection of chemical damage in concrete using ultrasound," *Ultrasonics*, vol. 40, nos. 1–8, pp. 247–251, May 2002.

[18] E. Ohdaira and N. Masuzawa, "Water content and its effect on ultrasound propagation in concrete—The possibility of NDE," *Ultrasonics*, vol. 38, nos. 1–8, pp. 546–552, Mar. 2000.

[19] Z. Lafhaj, M. Goueygou, A. Djerbi, and M. Kaczmarek, "Correlation between porosity, permeability and ultrasonic parameters of mortar with variable water/cement ratio and water content," *Cement Concrete Res.*, vol. 36, no. 4, pp. 625–633, Apr. 2006.

[20] T. Chady and P. Lopato, "Flaws identification using eddy current differential transducer and artificial neural networks," in *Proc. AIP Conf.*, vol. 820, no. 1. College Park, MD, USA: American Institute of Physics, 2006, pp. 783–790.

[21] T. Chady and M. Enokizono, "Multi-frequency exciting and spectrogram-based ECT method," *J. Magn. Magn. Mater.*, vol. 215, pp. 700–703, Jun. 2000.

[22] P. K. Frankowski, "Eddy current method for identification and analysis of reinforcement bars in concrete structures," in *Proc. Electrodynamic Mech. Syst.*, Oct. 2011, pp. 105–108.

[23] Ł. Drobiec, R. Jasiński, and W. Mazur, "Accuracy of eddy-current and radar methods used in reinforcement detection," *Materials*, vol. 12, no. 7, p. 1168, Apr. 2019.

[24] M. AbdelHafeez, A. H. Ahmed, and M. AbdelRaheem, "Design and operation of a lightweight educational testbed for Internet-of-Things applications," *IEEE Internet Things J.*, vol. 7, no. 12, pp. 11446–11459, Dec. 2020.

[25] C. A. Tokognon, B. Gao, G. Y. Tian, and Y. Yan, "Structural health monitoring framework based on Internet of Things: A survey," *IEEE Internet Things J.*, vol. 4, no. 3, pp. 619–635, Jun. 2017.

[26] G. Heo and J. Jeon, "A smart monitoring system based on ubiquitous computing technique for infra-structural system: Centering on identification of dynamic characteristics of self-anchored suspension bridge," *KSCE J. Civil Eng.*, vol. 13, no. 5, pp. 333–337, Sep. 2009.

[27] A. Myers, M. A. Mahmud, A. Abdelgawad, and K. Yelamarthi, "Toward integrating structural health monitoring with Internet of Things (IoT)," in *Proc. IEEE Int. Conf. Electro Inf. Technol. (EIT)*, May 2016, pp. 438–441.

[28] S. Panthati and A. Kashyap, "Design and implementation of structural health monitoring based on IoT using lab VIEW," *Int. J. Mag. Eng. Technol. Manag. Res.*, vol. 3, no. 2, pp. 77–82, 2016.

[29] S. Pandey, M. Haider, and N. Uddin, "Design and implementation of a low-cost wireless platform for remote bridge health monitoring," *Int. J. Emerg. Technol. Adv. Eng.*, vol. 6, no. 6, pp. 57–62, 2016.

[30] H. Malik, K. S. Khattak, T. Wiqar, Z. H. Khan, and A. B. Altamimi, "Low cost Internet of Things platform for structural health monitoring," in *Proc. 22nd Int. Multitopic Conf. (INMIC)*, Nov. 2019, pp. 1–7.

[31] F. Civerchia, S. Bocchino, C. Salvadori, E. Rossi, L. Maggiani, and M. Petracca, "Industrial Internet of Things monitoring solution for advanced predictive maintenance applications," *J. Ind. Inf. Integr.*, vol. 7, pp. 4–12, Sep. 2017.

[32] J. Wang, Y. Fu, and X. Yang, "An integrated system for building structural health monitoring and early warning based on an Internet of Things approach," *Int. J. Distrib. Sensor Netw.*, vol. 13, no. 1, 2017, Art. no. 1550147716689101.

[33] R. Igreja and C. J. Dias, "Analytical evaluation of the interdigital electrodes capacitance for a multi-layered structure," *Sens. Actuators A, Phys.*, vol. 112, nos. 2-3, pp. 291–301, May 2004.

[34] R. Igreja and C. J. Dias, "Extension to the analytical model of the interdigital electrodes capacitance for a multi-layered structure," *Sens. Actuators A, Phys.*, vol. 172, no. 2, pp. 392–399, Dec. 2011.

[35] S. O. P. Blume, R. Ben-Mrad, and P. E. Sullivan, "Modelling the capacitance of multi-layer conductor-facing interdigitated electrode structures," *Sens. Actuators B, Chem.*, vol. 213, pp. 423–433, Jul. 2015.

[36] G. Ghione and M. Goano, "Revisiting the partial-capacitance approach to the analysis of coplanar transmission lines on multilayered substrates," *IEEE Trans. Microw. Theory Techn.*, vol. 51, no. 9, pp. 2007–2014, Sep. 2003.

[37] C. Veyres and V. F. Hanna, "Extension of the application of conformal mapping techniques to coplanar lines with finite dimensions," *Int. J. Electron.*, vol. 48, no. 1, pp. 47–56, 1980.

[38] S. S. Gevorgian, "Basic characteristics of two layered substrate coplanar waveguides," *Electron. Lett.*, vol. 30, no. 15, pp. 1236–1237, Jul. 1994.

[39] N. H. Zhu, E. Y. B. Pun, and J. X. Li, "Analytical formulas for calculating the effective dielectric constants of coplanar lines for OIC applications," *Microw. Opt. Technol. Lett.*, vol. 9, no. 4, pp. 229–232, Jul. 1995.

[40] S. S. Gevorgian, T. Martinsson, P. L. J. Linner, and E. L. Kollberg, "CAD models for multilayered substrate interdigital capacitors," *IEEE Trans. Microw. Theory Techn.*, vol. 44, no. 6, pp. 896–904, Jun. 1996.

[41] (Aug. 25, 2021). *SIMULIA, CST Studio Suite*. [Online]. Available: https://www.3ds.com/products-services/simulia/products/cst-studio-suite/

[42] (Aug. 25, 2021). *ESP 8266-12 WiFi Module*. [Online]. Available: https://www.espressif.com/en/products/socs/esp8266

[43] (Aug. 25, 2021). *Atmel SAM3X8E ARM Cortex-M3*. [Online]. Available: http://ww1.microchip.com/downloads/en/DeviceDoc/Atmel-11057-32-bit-Cortex-M3-Microcontroller-SAM3X-SAM3A_Datasheet.pdf

[44] (Aug. 25, 2021). *ADNS-3050 Optical Sensor*. [Online]. Available: https://media.digikey.com/pdf/data%20sheets/avago%20pdfs/adns-3050.pdf

MOHAMED ABDELRAHEEM (Member, IEEE) received the B.Sc. and M.Sc. degrees in electrical engineering from Assiut University, Egypt, in 2004 and 2010, respectively, and the Ph.D. degree in electrical engineering from Virginia Tech, Blacksburg, VA, USA, in 2015. He is currently an Associate Professor of electrical engineering with Assiut University. His research interests include wireless networking, the Internet of Things, and embedded systems design and structural health monitoring. He has been a PI and a Co-PI for a number of research projects from Egyptian funding entities, such as STIFA, NTRA, and ITIDA. He is also a Royal Academy of Engineering-Leaders in Innovations Fellow. He has been serving as a reviewer for a number of IEEE conferences and journals.

AMR NASSR received the B.Sc. degree in civil engineering from Assiut University, Egypt, in 2004, and the M.A.Sc. and Ph.D. degrees in structural engineering from McMaster University, Hamilton, ON, Canada, in 2008 and 2012, respectively. He is currently an Associate Professor with the Faculty of Sustainable Design Engineering, Universities of Canada in Egypt, and the Department of Civil Engineering, Assiut University. His research interests include structural health monitoring of structures and resiliency of critical infrastructures exposed to multiple hazards. He is also a member of many professional societies, including the Professional Engineers of Ontario (PEO) and the Canadian Society of Civil Engineers (CSCE). He is also a Former of NSERC, a fellow of JSPS, and a Holder of many awards, including the Queen Elizabeth II Award in Science and Technology and International Excellence Award.

• • •

MAHMOUD ABDELHAFEEZ (Student Member, IEEE) received the B.Sc. and M.Sc. degrees in electrical engineering from Assiut University, in 2013 and 2020, respectively. He is currently pursuing the Ph.D. degree with Carleton University, Ottawa, ON, Canada. He has been working as a Teaching and Research Assistant with the Electrical Engineering Department, Assiut University, since 2015. His current research interests include the Internet of Things networks and security, WSNs, analysis and design of hardware-secured algorithms, side-channel analysis, and embedded systems security and solutions.